PERGAMON

International Journal of Solids and Structures 38 (2001) 6907–6924

INTERNATIONAL JOURNAL OF SOLIDS and STRUCTURES

www.elsevier.com/locate/ijsolstr

Numerical analysis of directionally unstable crack propagation in adhesively bonded joints

Buo Chen [1], David A. Dillard *

Department of Engineering Science and Mechanics, Virginia Polytechnic Institute and State University, Blacksburg, VA 24061-0219, USA

Received 15 March 2000

Abstract

This paper investigates the directional stability of crack propagation in adhesively bonded joints. First, an analytical model analyzing the energy balance during the crack propagation in double cantilever beam specimens is presented, and the directional stability of cracks is predicted. The results are consistent with the predictions made by Fleck, Hutchinson, and Suo (Int. J. Solids Struct. 27 (13) (1991) 1683) using a stress analysis approach, and also are consistent with experimental observations. Similar to the situation in homogeneous solids, cracks in adhesively bonded joints also tend to be directionally unstable when the *T*-stress is positive (tensile) whereas tend to be directionally stable when the *T*-stress is negative (compressive). Both interface mechanics and the finite element method are then employed to analyze the stress state at the crack tip and to predict crack trajectories. Through extending the criteria for direction of crack propagation to bi-material systems, the trajectory for directionally unstable cracks is simulated. The simulation result accurately reflects the alternating nature of directionally unstable cracks in adhesive bonds such as the characteristic length and the overall shape. © 2001 Published by Elsevier Science Ltd.

Keywords: Directional stability of cracks; Locus of failure; Direction of crack propagation; Crack path selection; Adhesively bonded joints; *T*-stress; Mixed mode fracture; Interface crack

1. Introduction

Characterizing crack propagation behavior is an important aspect in investigating the fundamental mechanism of crack path selection in adhesively bonded joints (Fleck et al., 1991; Chai, 1987; Dillard et al., 1998; Chen and Dillard, 2001). In conventional theories of fracture mechanics, the onset of fracture for a crack is characterized by a single parameter. Under predominantly elastic conditions, the controlling parameter is the stress intensity factor K or the strain energy release rate G. When yielding is more widespread, the parameter is either the J-integral (Rice, 1968; Hutchinson, 1968), or the crack opening displacement

* Corresponding author. Tel.: +1-540-231-4714; fax: +1-540-231-9187.
E-mail address: dillard@vt.edu (D.A. Dillard).
[1] Current address: Cooper Tire and Rubber Co., 701 Lima Avenue, Findlay, OH 45840, USA.

0020-7683/01/$ - see front matter © 2001 Published by Elsevier Science Ltd.
PII: S0020-7683(01)00006-3

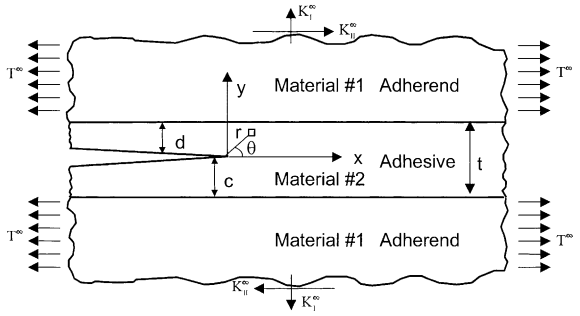

Fig. 1. A crack within the adhesive layer in an adhesive bond. The adherend is designated as material 1 and adhesive is designated as material 2. The coordinate system is set at the crack tip.

(Broek, 1982). However, other details of the crack propagation behavior such as the direction of cracking and the directional stability of cracks require more information of the stress state at the crack tip.

According to Williams (1957) and Westergaard (1939), if a Cartesian coordinate is set at the crack tip with the x-axis pointing along the crack plane as shown in Fig. 1, the stress distribution at the crack tip in homogeneous solids is given by

$$\begin{bmatrix} \sigma_{xx} & \sigma_{xy} \\ \sigma_{xy} & \sigma_{yy} \end{bmatrix} = \frac{K_I}{\sqrt{2\pi r}} \cos\left(\frac{\theta}{2}\right) \begin{bmatrix} 1 - \sin\left(\frac{\theta}{2}\right)\sin\left(\frac{3\theta}{2}\right) & \sin\left(\frac{\theta}{2}\right)\sin\left(\frac{3\theta}{2}\right) \\ \sin\left(\frac{\theta}{2}\right)\sin\left(\frac{3\theta}{2}\right) & 1 + \sin\left(\frac{\theta}{2}\right)\sin\left(\frac{3\theta}{2}\right) \end{bmatrix} + \frac{K_{II}}{\sqrt{2\pi r}} \begin{bmatrix} -\sin\left(\frac{\theta}{2}\right)\left[2 + \cos\left(\frac{\theta}{2}\right)\cos\left(\frac{3\theta}{2}\right)\right] & \cos\left(\frac{\theta}{2}\right)\left[1 - \sin\left(\frac{\theta}{2}\right)\sin\left(\frac{3\theta}{2}\right)\right] \\ \cos\left(\frac{\theta}{2}\right)\left[1 - \sin\left(\frac{\theta}{2}\right)\sin\left(\frac{3\theta}{2}\right)\right] & \sin\left(\frac{\theta}{2}\right)\cos\left(\frac{\theta}{2}\right)\cos\left(\frac{3\theta}{2}\right) \end{bmatrix} + \begin{bmatrix} T & 0 \\ 0 & 0 \end{bmatrix} + O(\sqrt{r}) \tag{1}$$

In Eq. (1), r and θ are the polar coordinates, and K_I and K_{II} are the mode I and mode II stress intensity factors, respectively.

As reviewed in Chen and Dillard (2001), the direction of crack propagation is closely related to the stress and energy state at the crack tip. To determine the direction of cracking, three criteria have been commonly discussed in the literature: (1) Maximum opening stress criterion by Ergodan and Sih (1963). This criterion dictates that the direction of cracking is perpendicular to the direction of maximum opening stress at the crack tip. (2) Maximum energy release rate criterion by Palaniswamy and Knauss (1978). Through applying this criterion, the direction of crack propagation can be obtained by maximizing the energy release rate as a function of the angle of crack kinking. (3) Mode I fracture criterion by Goldstein and Salganik (1974) and Cotterell and Rice (1980). According to this criterion, a crack will propagate along a path such that pure mode I fracture is maintained at the crack tip, i.e. $K_{II} = 0$ at the crack tip. According to Palaniswamy and Knauss (1878), and Hutchinson and Suo (1992), the results obtained using any one of these three criteria are very similar and no distinguishable experimental differences have been observed; therefore, the choice of criterion in practice totally depends on convenience.

These criteria, although developed primarily for cracks in homogeneous materials, can be readily extended into bi-material systems such as adhesively bonded joints according to Hutchinson and Suo (1992). However, care should be used when applying these criteria to determine the direction of cracking for cracks located at a bi-material interface due to differences in fracture toughness in the vicinity of an interface. Further details associated with the determination of the direction of cracking in adhesive bonds using these criteria are discussed in the analyses of this paper.

In investigating slightly curved or kinked cracks, Cotterell and Rice (1980) indicated the importance of the T term in Eq. (1), which is non-singular and acts parallel to the crack plane. Although this T-stress is much smaller than the singular terms at the crack tip, its magnitude is closely related to the directional stability of cracks. According to Cotterell and Rice (1980), cracks tend to be directionally unstable if the T-stress is positive (tensile) and directionally stable if the T-stress is negative (compressive). Through considering higher order terms in the Williams (1957) asymptotic stress expansion for a crack in a homogeneous solid, Chao and Liu (1997) and Zhu and Chao (2001) further investigated the effect of the T-stress on the crack propagation manner. The results indicate that the direction of the maximum opening stress at a crack tip varies with the T-stress level and consequently, so does the direction of cracking according criterion (1). The study of Chao and Liu (1997) and Zhu and Chao (2001) provides further insights into understanding the effect of the T-stress on the crack propagation behavior in homogeneous media. Not only the directional stability of cracks, but also the direction of crack propagation will be affected by the T-stress. Chao and Liu (1997) and Zhu and Chao (2001) also clarified that although the criteria for direction of cracking and directional stability of cracks are developed under the assumptions of linear fracture mechanics, they are still applicable for ductile materials in most cases.

In adhesively bonded systems, the issue of directional stability of cracks was first discussed by Chai (1984, 1986, 1987), who observed a unique form of crack trajectory in the mode I delamination failure of graphite reinforced epoxy composite laminates and aluminum/epoxy bonds. Overall, the crack periodically alternated between the two interfaces with a characteristic length of three to four times the thickness of the adhesive layer. More specifically, as the crack advanced, the crack propagated along one interface and then gradually deviated away with an increasing slope until the other interface was approached. An abrupt kink then occurred when the crack approached the opposite interface. The crack then propagated near the interface for a distance of about two to three times the thickness of the adhesive layer before deviating from the interface again. As a result, a characteristic length of three to four times the thickness of the adhesive was observed in the crack trajectory. This trajectory obviously reflects very directionally unstable crack propagation. Fleck et al. (1991) and Akisanya and Fleck (1992a) investigated this directional stability issue analytically and indicated that, as with homogeneous materials, the directional stability of cracks in adhesively bonded joints also depends on the T-stress level. Cracks in adhesive bonds also tend to be directionally stable if the T-stress is negative and tend to be directionally unstable if the T-stress is positive.

For an adhesive bond of sandwich geometry with semi-infinite adherends as shown in Fig. 1, Fleck et al. (1991) obtained the T-stress as

$$T = \frac{1-\alpha}{1+\alpha} T^{\infty} + \sigma_0 + C_{\mathrm{I}}(c/t, \alpha, \beta) \frac{K_{\mathrm{I}}^{\infty}}{\sqrt{t}} + C_{\mathrm{II}}(c/t, \alpha, \beta) \frac{K_{\mathrm{II}}^{\infty}}{\sqrt{t}} \tag{2}$$

where σ_0 is the residual stress in the adhesive and t is the thickness of the adhesive layer. K_{I}^{∞}, K_{II}^{∞}, and T^{∞} in Eq. (2) are solutions for homogeneous material specimens obtained by neglecting the adhesive layer in the geometry and here they are used as far field loading. The manner in which K_{I}^{∞} and K_{II}^{∞} are related to specific applied loading can be found in Tada et al. (1985). T^{∞} has been obtained by Larsson and Carlsson (1973) for several commonly used testing geometries. $C_{\mathrm{I}}(c/t, \alpha, \beta)$ and $C_{\mathrm{II}}(c/t, \alpha, \beta)$ in Eq. (2) are non-dimensional functions tabulated in Fleck et al. (1991), c is the distance between the crack and the interface as shown in Fig. 1, and α and β are Dundurs' parameters indicating the material mismatch, which are defined as

$$\begin{aligned} \alpha &= \frac{\mu_1(\kappa_2+1) - \mu_2(\kappa_1+1)}{\mu_1(\kappa_2+1) + \mu_2(\kappa_1+1)} \\ \beta &= \frac{\mu_1(\kappa_2-1) - \mu_2(\kappa_1-1)}{\mu_1(\kappa_2+1) + \mu_2(\kappa_1+1)} \end{aligned} \tag{3}$$

where the subscripts 1 and 2 refer to the materials for the adherends and adhesive, respectively; μ_i $(i = 1, 2)$ are shear moduli; $\kappa_i = 3 - 4\nu_i$ with $i = 1, 2$ for plane strain and $\kappa_i = (3 - \nu_i)/(1 + \nu_i)$ for plane stress; and ν_i $(i = 1, 2)$ are the Poisson's ratios. The value of α is between -1 and 1, and according to Suga et al. (1988) and Fleck et al. (1991), the value of β is between 0 and $\alpha/4$ for most material combinations. For specimens with monolithic material, the T-stresses, which is the T^{∞} in Eq. (2), for several commonly used testing geometries such as the compact tension, bending, and double cantilever beam (DCB) specimens are positive according to Larsson and Carlsson (1973). When an adhesive layer with lower modulus than the adherends is introduced, then the T-stress in the specimen may become negative due to the material mismatch as indicated in Eq. (3). To study the crack path selection in adhesively bonded joint, the DCB specimen geometry has been commonly used since the geometry provides a relatively long testing window as compared to other geometries such as the compact tension and bending specimens. In addition, the preparation of the DCB specimens including the surface treatment and curing process is relatively convenient.

Chen and Dillard (2001) experimentally demonstrated the T-stress dependence of the directional stability of cracks in adhesive bonds through mechanically altering the T-stress levels in DCB specimens. In their tests, the adhesive used was an epoxy resin with 8.1% rubber concentration in weight and the adherends were aluminum alloy 6061-T6. After bonding, the DCB specimens were loaded uniaxially until the adherends were plastically deformed. Due to the plastic deformation in the adherends, the residual stresses in the adhesive layer were increased, and so was the T-stress due to the relationship between the T-stress and the residual stress. Details of the experimental procedure and the T-stress calculations for DCB specimens can be found in Chen and Dillard (2001).

Concerns have been raised whether any microcracks in the adhesive layer were induced during the stretching procedure. This issue is critical because the crack propagation behavior and resulting trajectory might be influenced by the microcracks. To further investigate the stretching processes, blue fountain pen ink was applied to both sides of the DCB specimens while they were being stretched. Due to the surface energy, the ink should wick into the microcracks as soon as they formed. The experiments showed no evidence of ink wicking before the maximum strain approached 2.1% and when the maximum strain was beyond 2.1%, ink wicking was observed in some specimens. This experimental result indicated that no microcrack should be induced during the stretching process as long as the total strain is controlled to be less than 2.1% for this particular material system, and the highest strain level concerned herein is about 1.9%.

After the specimens were prepared, they were then tested under quasi-static mode I loading, and the crack trajectories in the specimens showed that cracks in as-produced specimens were directionally stable, but tended to be more and more directionally unstable as the plastic deformation level increased, which verified the predictions made by Fleck et al. (1991) of the T-stress dependence of the directional stability of cracks. Chen and Dillard (2001) also showed that the solution for T-stress obtained by Fleck et al. (1991) as shown in Eq. (2) in fact is the lower bound of the T-stress for DCB specimens since the adherends were assumed to be semi-infinite in their analysis. As the thickness of adherends decreases, the effect of adherend bending becomes more pronounced. As a result, the magnitude of the T-stress increases slightly. This adherend bending effect indicates that the crack tends to be more directionally unstable as the thickness of adherends decreases, which was also experimentally verified in Chen and Dillard (2001) using DCB specimens with different adherend thicknesses.

Shown in Fig. 2 is a typical micrograph of the directionally unstable crack trajectory observed, which was taken from the cross-section of a DCB specimen after failure. The scanning electron micrograph (SEM) insert reveals several characteristics in the crack trajectory that are very similar to what Chai (1984, 1986, 1987) observed: (a) The crack trajectory periodically alternates between the interfaces with a characteristic length of three to four times the thickness of the adhesive layer. (b) Along the direction of crack propagation, the crack always deviates from the interface gradually with an increasing slope until the opposite interface is approached. (c) An abrupt kink occurs when the crack approaches the opposite interface and the crack then stays at the sub-interface. (d) The crack deviates from the interface again after propagating

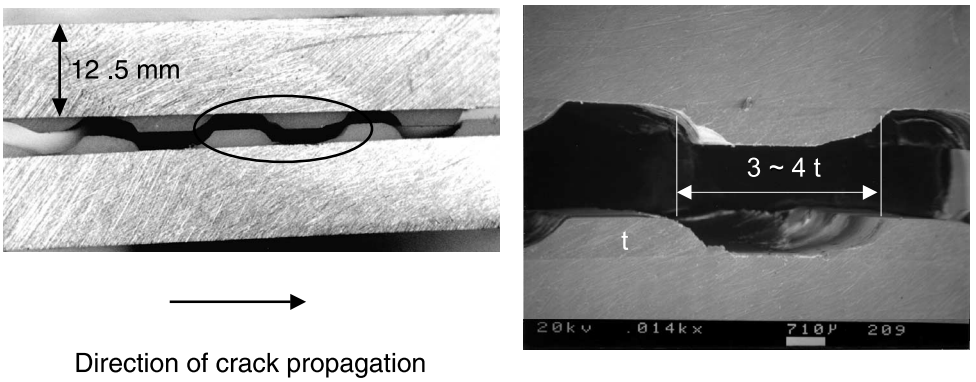

Fig. 2. The cross-section of the failed specimen with $T = 35$ MPa and alternating crack trajectory. The picture on the right is the SEM of the circled portion of the cross-section.

at the sub-interface for a distance about two to three times the thickness of the adhesive. (e) The crack trajectory overall appears to be antisymmetric with the centerline of the adhesive bond along the direction of crack propagation.

Akisanya and Fleck (1992a,b) analyzed the crack trajectory Chai (1984, 1986, 1987) reported using an idealized crack geometry resembling the "square wave". The specimen was replaced by a circular domain of radius R that is much greater than the adhesive thickness t, and the remote loads were replaced by $K^{\infty} = K_{\mathrm{I}}^{\infty} + \mathrm{i}K_{\mathrm{II}}^{\infty}$ as shown in Fig. 3. The analysis showed that the crack would kink out of the interface when the interfacial crack length L reached a characteristic length L_{c} where the local stress intensity factor is high enough and the phase angle equals the critical interfacial phase angle indicated in He and Hutchinson (1989). Furthermore, the characteristic length L_{c} was related to the Dundurs' parameters α and β, the thickness of the adhesive layer t, residual stress σ_0, and the interface toughness. Using the finite element method, Chen et al. (2001) later simulated the directionally unstable crack trajectories in DCB specimens

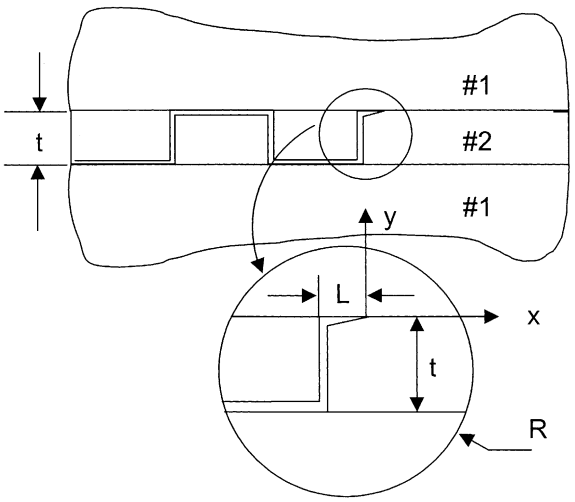

Fig. 3. The idealized crack trajectory geometry used in Akisanya and Fleck (1992a,b).

for different material systems, which further explored the material system dependence of the characteristic length of directionally unstable cracks.

In this paper, an analytical model is introduced to assess the energy balance during crack propagation in the DCB specimens studied in Chen and Dillard (2001). Using the energy model, the directional stability of cracks is predicted, and the results are consistent with the predictions in Fleck et al. (1991) made using a stress analysis approach, and also consistent with the experimental observations in Chai (1987) and Chen and Dillard (2001). Both interface mechanics and numerical analysis using the finite element method are then employed to analyze the stress state at the crack tip and to predict the crack path. Extending the criteria for the direction of cracking to a bi-material system, the trajectory for directionally unstable cracks is simulated. The simulation result accurately reflected the alternating nature of directionally unstable cracks in adhesive bonds such as the characteristic length and the overall shape of the crack.

2. Energy balance and directional stability of crack propagation

Because of the thermal mismatch, a residual stress is induced during the fabrication of adhesive bonds. If the residual stress is released, the stored strain energy will be reduced. Compared to a directionally stable crack where the crack trajectory is fairly straight, Fig. 2 shows that due to the alternating feature, more residual stress is released in the directionally unstable crack propagation, and consequently, a greater amount of energy is available to propagate the crack. On the other hand, because the crack trajectory is more tortuous, the crack propagates along a longer crack path when the crack is directionally unstable, which indicates that more energy is consumed during the fracture process. This close relationship between the manner of crack propagation and the energy flow in the system suggests that the directional stability of cracks in adhesive bonds can be predicted through analyzing the energy balance in the system. An energy balance model was therefore constructed to predict the directional stability of cracks in the DCB specimens tested in Chen and Dillard (2001).

Shown in Fig. 4 is the DCB specimen analyzed with an alternating crack in the bond. The crack trajectory is idealized resembling a "square wave" similar to that in Akisanya and Fleck (1992a,b), and the purpose of the analysis is to determine the energy available for the alternating crack propagation. Although the simplification of the crack trajectory is rather crude since many details are ignored, the error induced is essentially negligible as far as energy flows are concerned because the model only contains about a 5% error in the total length of the crack trajectory and the total area of the additional free surfaces associated with the release of residual stress. The material system analyzed was the same as that in Chen and Dillard (2001). The adherends designated as material 1 are aluminum, having a Young's modulus of $E_1 = 70$ GPa and Poisson's ratio of $v_1 = 0.33$. The adhesive, designated as material 2, represents an epoxy and has a modulus of $E_2 = 2.97$ GPa, Poisson's ratio of $v_2 = 0.33$, and thickness of $t = 0.5$ mm.

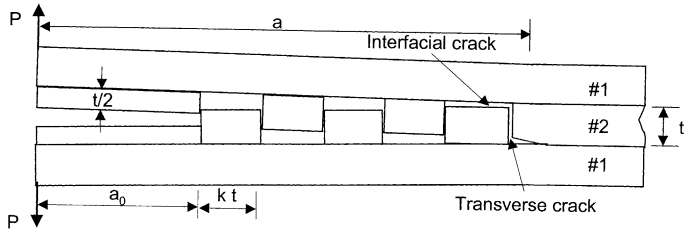

Fig. 4. A DCB specimen with simplified crack trajectory for directionally unstable crack propagation.

To further simplify the analysis, several other assumptions were made: (a) According to the results in Chen and Dillard (2001), the measured fracture toughness of the aluminum/epoxy bonds is approximately independent of the directional stability of cracks for this materials system studied based on the plane area of the specimens; therefore, the specimens are assumed to have a single critical fracture toughness value $G_c = 310$ J/m^2, which was obtained from the quasi-static DCB tests of as-produced specimens. (b) Loads are applied at one end of the specimens. (c) The adherends are stiff compared to the adhesive; therefore, in the failed portion of the specimen, the adherend bending due to the residual stress in the adhesive is negligible. For the same reason, the effect of the adhesive layer on the flexural rigidity of the specimens is negligible.

For the crack trajectory shown in Fig. 4, the energy available during the fracture process consists of two parts, U_1 and U_2. U_1 is the strain energy available when the crack propagates along the interfaces and U_2 is the strain energy available for the transverse crack propagation. U_1 is the same as the energy available during the directionally stable crack propagation according the iso-fracture toughness assumption and can be obtained using the conventional compliance analysis as

$$U_1 = \frac{a^3 P^2}{3E_1 I_1} \tag{4}$$

where a is the crack length, $E_1 I_1$ is the effective flexural rigidity of the DCB specimen, and P is the load. I_1 is estimated as

$$I_1 = \frac{B(t/2)^3}{12} + B\frac{t}{2}\left(\frac{t}{4} + d'\right)^2 + \frac{nBH^3}{12} + nBH\left(\frac{H}{2} - d'\right)^2 \tag{5}$$

where t is the thickness of the adhesive layer, B is the width of the specimen, H is the thickness of the adherends, $n = E_1/E_2$ is the modulus ratio of the adherend versus the adhesive, and d' is given by

$$d' = \frac{4nH^2 - t^2}{4t + 8nH} \tag{6}$$

Under the iso-fracture toughness assumption, P in Eq. (4) is given by

$$P = \frac{\sqrt{G_c B E I_1}}{a} \tag{7}$$

If the adherends are much stiffer than the adhesive as stated in assumption (c), the effect of the adhesive layer on the flexural rigidity of the DCB specimen is negligible and $I_1 \cong BH^3/12$. If the thickness of the adherends decreases as that in T-peel specimens, the effect of the adhesive layer on the flexural rigidity of the specimen is no longer negligible and Eq. (5) should be used.

To calculate the strain energy U_2, a single transverse crack is isolated as shown in Fig. 5 and the strain energy u available for this particular crack is given by

$$u = \frac{\sigma}{2}\int_0^t \delta(y)\,\mathrm{d}y \tag{8}$$

where $\delta(y)$ is the crack opening displacement profile and σ is the stress distributed along the crack surfaces prior to cracking. If the crack is assumed to be a Griffith crack as Suo (1990) and Nairn (1989) suggested in studying tunneling cracks in coatings and composites, $\delta(z)$ under plane-strain conditions is given by

$$\delta(y) = 4\sigma\frac{1 - \nu_2^2}{E_2}\sqrt{y^2 - z^2} \tag{9}$$

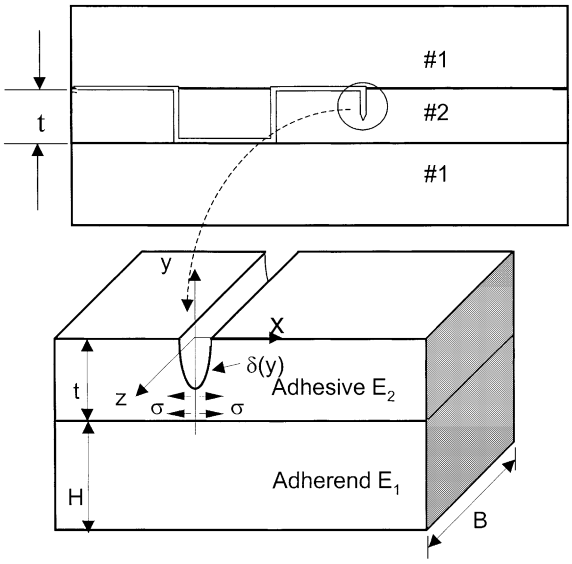

Fig. 5. The geometry and the stress state of a transverse crack in the DCB specimen with simplified crack trajectory for directionally unstable crack propagation.

The choice of $\delta(z)$ was also verified by the finite element analysis conducted to investigate the geometry of a vertical opening crack in an adhesively bonded DCB specimen. Substituting Eq. (9) into Eq. (8) and using Fig. 4, the strain energy available for transverse crack propagation U_2 is then obtained as

$$U_2 = \frac{\pi}{2}\left(\frac{a - a_0 + kt}{2kt}\right)\left(\frac{1 - v_2^2}{E_2}\right)B\sigma^2 t^2 \tag{10}$$

where a_0 is the precrack length as shown in Fig. 4, kt is the characteristic length of the alternating crack trajectory, and the opening stress applied at the crack surfaces σ is still to be determined.

The normal stress, σ, depends on the residual stress in the adhesive, specimen geometry, and the external loads. Setting the coordinate system as shown in Fig. 5, plane-stress prevails when investigating the stress state in the adhesive layer because the normal stress $\sigma_y = 0$ due to the viscoelastic properties of the adhesive. Therefore, according to assumption (c), the constitutive equation for the adhesive is given by

$$\begin{aligned}\varepsilon_x &= (\alpha_1 - \alpha_2)(T_{\mathrm{sft}} - T_t) + \frac{1}{E_2}(\sigma_x - v\sigma_z)\\ \varepsilon_z &= (\alpha_1 - \alpha_2)(T_{\mathrm{sft}} - T_t) + \frac{1}{E_2}(\sigma_z - v\sigma_x)\end{aligned} \tag{11}$$

where ε_x and ε_z are the total strain of the adhesive, T_{sft} is the stress free temperature of the adhesive, which is very close to the glass transition temperature for the adhesive studied according to Chen and Dillard (2001), T_t is the test temperature (room temperature in this case), and α_1 and α_2 are coefficients of thermal expansion (CTE) for the adherend and the adhesive, respectively. During the fabrication of the specimens, an equal, bi-axial residual stress σ_0 is induced in the curing procedure due to the CTE mismatch and can be obtained using Eq. (11) as

$$\sigma_0 = \frac{E_2}{1 - v_2}(\alpha_2 - \alpha_1)(T_{\mathrm{sft}} - T_t) \tag{12}$$

The residual stress estimated using Eq. (12) is about 13 MPa for this material system, which is consistent with the experimental results from a curvature measurement technique using aluminum/epoxy bi-material strips. Details of the residual stress measurement technique can be found in Dillard et al. (1999b).

If the specimens were stretched uniaxially until the adherends were plastically deformed before test in order to vary the residual stress, and consequently the T-stress as discussed in Chen and Dillard (2001), the bi-axial stresses induced due to the plastic deformation in the adherends are given by

$$\begin{aligned}\sigma'_x &= \frac{E_2}{(1-v_2^2)}(1-v_2v_1)\varepsilon_{\mathrm{p}} \\ \sigma'_y &= \frac{E_2}{(1-v_2^2)}(v_2-v_1)\varepsilon_{\mathrm{p}}\end{aligned} \tag{13}$$

where ε_{p} is the plastic deformation that occurred in the adherends during the stretching. This result is consistent with that Dillard et al. (1999a) obtained in studying the stress state of coatings subjected to similar combinations of biaxial residual plus uniaxial extension stresses.

When the DCB specimen is loaded during testing, an additional normal stress σ''_x is induced at the crack surfaces prior to cracking due to the bending of the adherends and is given by

$$\sigma''_x = \frac{Pa(t/2+d)}{I_1} \tag{14}$$

where d is given by

$$d = \frac{nH^2 - t^2}{2(t+nH)} \tag{15}$$

Combining Eqs. (12)–(14), the stress σ applied at the transverse crack surfaces can be obtained as

$$\sigma = \frac{Pa(t/2+d)}{I_1} + \frac{E_2}{1-v_2}(\alpha_2-\alpha_1)(T_{\mathrm{sft}}-T_t) + \frac{E_2}{(1-v_2^2)}(1-v_2v_1)\varepsilon_{\mathrm{p}} \tag{16}$$

Substituting Eq. (16) into Eq. (10), the strain energy available for the transverse crack propagation is then obtained. Dividing the total strain energy $U = U_1 + U_2$ by the total crack area, the average strain energy release rate for the crack propagation is obtained.

Shown in Fig. 6 is the result of the analysis. The ordinate of the figure is the normalized average strain energy release rate with respect to the critical strain energy release rate G_{c} ($= 310$ J/m^3) of the DCB specimens tested in Chen and Dillard (2001), and the abscissa represents the thickness of the adherends.

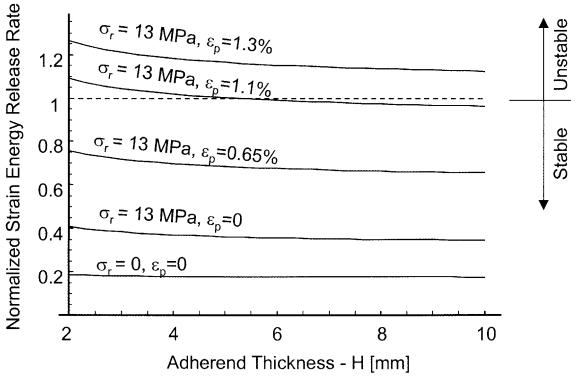

Fig. 6. Available strain energy release rate for directionally unstable crack propagation in DCB specimen with various conditions.

The dashed line represents the critical strain energy release rate for the alternating crack propagation and therefore, also represents the threshold of the transition of the directional stability of the crack propagation. If the available strain energy release rate is higher than the critical strain energy release rate for the alternating crack trajectory, cracks in the specimen are more likely to be directionally unstable since there is enough energy available for cracks to propagate along the alternating path. On the other hand, if the available strain energy release rate for the alternating crack propagation is lower than the critical strain energy release rate, cracks are more likely directionally stable. Fig. 6 shows that when the plastic deformation in the adherends ε_p is less than 1.1%, the curves are all below the dashed line indicating a likelihood for directionally stable crack propagation. As the plastic deformation ε_p in the adherends increases (consequently, the T-stress also increases), more strain energy becomes available and the curves shift upwards, suggesting an increase in the probability of directionally unstable cracks. This result is consistent quantitatively with the predictions made by Fleck et al. (1991) using the T-stress argument. Experimental results discussed in Chen and Dillard (2001) also indicated good consistency quantitatively with the predictions made by this energy balance model.

All curves in Fig. 6 are monotonically decreasing with increasing adherend thickness, indicating an effect of adherend bending on the directional stability of cracks. For instance, the curve with $\varepsilon_p = 1.3\%$ and $\sigma_0 = 13$ MPa is higher than the dashed line when H is less than 4 mm and is lower than the dashed line when H is greater than 4 mm. Since the dashed line represents the threshold of the directional stability of crack propagation, this curve indicates that for specimens with $\varepsilon_p = 1.3\%$ and $\sigma_0 = 13$ MPa, the directional stability of cracks varies with the thickness of the adherends. This prediction is also verified by the experimental results in Chen and Dillard (2001), where DCB specimens with adherend thicknesses H of 4.8 and 3.2 mm, respectively, were tested. The cracks in specimens with $H = 3.2$ mm were more directionally unstable than the cracks in specimens with $H = 4.8$ mm when the residual stresses and the plastic deformation levels were the same.

Fig. 6 also indicates an effect of the toughness of the adhesive bonds on the directional stability of cracks. When the toughness of the bond increases, all the curves will shift down vertically, indicating that the transition between the directionally stable and unstable crack is less likely to occur. More detailed discussion about the effect of the adhesive toughness can be found in Chen et al. (2001), where experimental results are also presented.

3. Interface mechanics and the prediction of crack trajectories

In this section, discussion focuses on the interface mechanics and the details of crack trajectory predictions. For a crack at the interface between the adherend and adhesive as shown in Fig. 7a, the stress distribution ahead of the crack $\theta = 0$ is characterized by Williams (1959) asymptotic stress expansion,

$$\sigma_{yy} + \mathrm{i}\sigma_{xy} = \frac{(K_1 + \mathrm{i}K_2) r^{\mathrm{i}\varepsilon}}{\sqrt{2\pi r}} \tag{17}$$

where $(r^{\mathrm{i}\varepsilon}/\sqrt{r}) = (1/\sqrt{r})\cos(\varepsilon \ln r) + (1/\sqrt{r})\,\mathrm{i}\sin(\varepsilon \ln r)$ is the oscillatory singularity characteristic of cracks at the interface between two dissimilar solids, K_1 and K_2 comprise the complex stress intensity factor analogous to the conventional stress intensity factors K_I and K_{II}, and ε is defined as

$$\varepsilon = \frac{1}{2\pi} \ln\left(\frac{1-\beta}{1+\beta}\right) \tag{18}$$

where β is the Dundurs' parameter.

If the crack lies below the interface a small distance δt instead of at the interface, as shown in Fig. 7b, the stresses ahead of the sub-interface crack tip ($\theta = 0$) are characterized by the conventional stress intensity factor K_I and K_{II} as

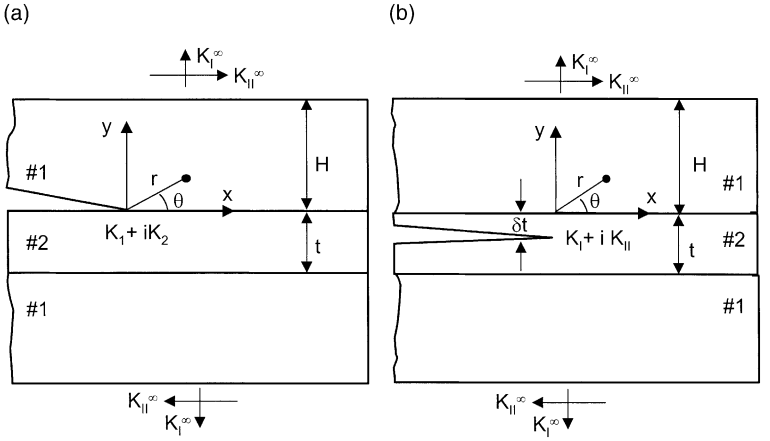

Fig. 7. Cracks in a DCB specimen: (a) interfacial crack and (b) cohesive crack. The specimen is under external K_{I}^{∞} and K_{II}^{∞} loading, which can also be described as far field stress intensity factors.

$$\sigma_{yy} + \mathrm{i}\sigma_{xy} = \frac{K_{\mathrm{I}} + \mathrm{i}K_{\mathrm{II}}}{\sqrt{2\pi r}} \tag{19}$$

According to Hutchinson et al. (1987), Hill et al. (1996), and Suo and Hutchinson (1989), the relation between the complex stress intensity factors, K_1 and K_2, and the conventional stress intensity factors, K_{I} and K_{II}, can be obtained through investigating of the global energy balance of the system as

$$K_{\mathrm{I}} + \mathrm{i}K_{\mathrm{II}} = q\mathrm{e}^{\mathrm{i}\phi}(K_1 + \mathrm{i}K_2)\delta t^{\mathrm{i}\varepsilon} \tag{20}$$

where $q = \sqrt{(1-\beta^2)/(1+\alpha)}$ is a real quantity and $\phi(\alpha,\beta)$ is a dimensionless function of the elastic moduli listed in Hutchinson and Suo (1992) for different material combinations. Eq. (20) requires the distance between the sub-interfacial crack and the interface δt to be small because the derivation is based on the assumption that the solution for the sub-interface crack approaches that of the interface crack when the distance from the crack tip is greater than δt according to Hutchinson et al. (1987).

According to Suo and Hutchinson (1989), similar arguments can be used to derive the relationship between the local complex stress intensity factors, K_1 and K_2, for the interface crack and the far field stress intensity factors, K_{I}^{∞} and K_{II}^{∞}, which are taken as the loading conditions, giving

$$K_1 + \mathrm{i}K_2 = p\left(K_{\mathrm{I}}^{\infty} + \mathrm{i}K_{\mathrm{II}}^{\infty}\right)t^{-\mathrm{i}\varepsilon}\mathrm{e}^{\mathrm{i}\omega(\alpha,\beta)} \tag{21}$$

where $p = \sqrt{(1-\alpha)/(1-\beta^2)}$, $\omega(\alpha,\beta)$ is a dimensionless functions of material constants and is also listed in Hutchinson and Suo (1992), and K_{I}^{∞} and K_{II}^{∞} is directly related to the external loads applied on the specimen and can be found in Tada, Paris, and Irwin (1985). Specifically, for symmetric DCB specimens, which are under predominantly mode I loading, the relationship is given by

$$K_{\mathrm{I}}^{\infty} + \mathrm{i}K_{\mathrm{II}}^{\infty} = K_{\mathrm{I}}^{\infty} = f\frac{Pa}{B}H^{-3/2}\left(2\sqrt{3} + 2.315\frac{H}{a}\right) \tag{22}$$

where P is the external load, B is the width of the specimen, a is the crack length, and f equals 1 for plane stress and $1/\sqrt{1-\nu_1^2}$ for plane strain. Substituting Eq. (22) into Eq. (21), the local complex stress intensity factors for an interface crack in a DCB specimen can be expressed as a function of the external load as

$$K_1 + \mathrm{i}K_2 = pf\frac{Pa}{B}H^{-3/2}\left(2\sqrt{3} + 2.315\frac{H}{a}\right)t^{-\mathrm{i}\varepsilon}\mathrm{e}^{\mathrm{i}\omega(\alpha,\beta)} \tag{23}$$

If the crack is at the sub-interface, the local stress intensity factor K_{I} and K_{II} can also be expressed as a function of the external load by substituting Eq. (23) into Eq. (20),

$$\begin{aligned} K_{\mathrm{I}} &= q|K|\cos\left[\omega + \phi + \varepsilon\ln(\delta t/t)\right] \\ K_{\mathrm{II}} &= q|K|\sin\left[\omega + \phi + \varepsilon\ln(\delta t/t)\right] \end{aligned} \tag{24}$$

where, $|K|$ is given by

$$|K| = pf\sqrt{GE_1/12}\left(2\sqrt{3} + 2.315\frac{H}{a}\right) \tag{25}$$

and $G = 12P^2a^2/E_1B^2H^3$ is the applied strain energy release rate in the specimen.

Figs. 8 and 9 show that due to the material mismatch, when the distance between the sub-interface crack and the interface δt is small, the corresponding K_{II} component at the crack tip is very high and is acting in

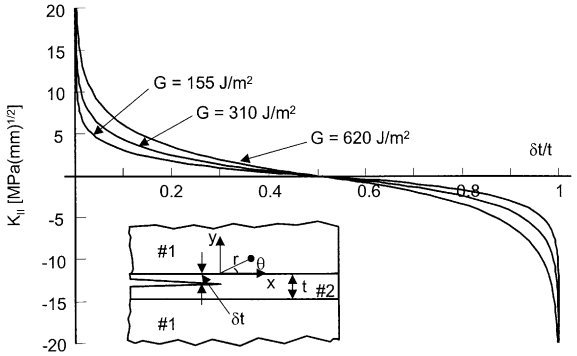

Fig. 8. The curve of local mode II stress intensity factor K_{II} versus the non-dimensional location of the sub-interfacial crack varies with the applied strain energy level.

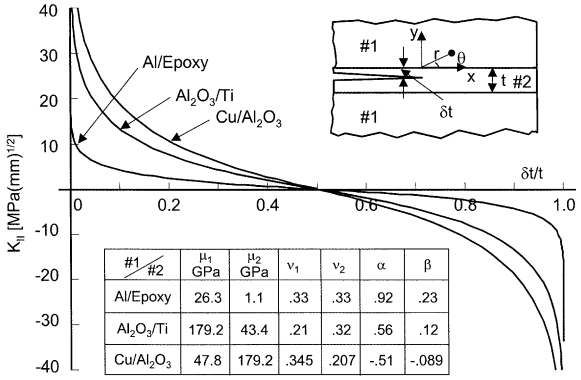

#1 / #2	μ_1 GPa	μ_2 GPa	ν_1	ν_2	α	β
Al/Epoxy	26.3	1.1	.33	.33	.92	.23
Al_2O_3/Ti	179.2	43.4	.21	.32	.56	.12
Cu/Al_2O_3	47.8	179.2	.345	.207	-.51	-.089

Fig. 9. Parametric study of the local mode II stress intensity factor K_{II} versus the non-dimensional location of the sub-interfacial crack for different material combinations.

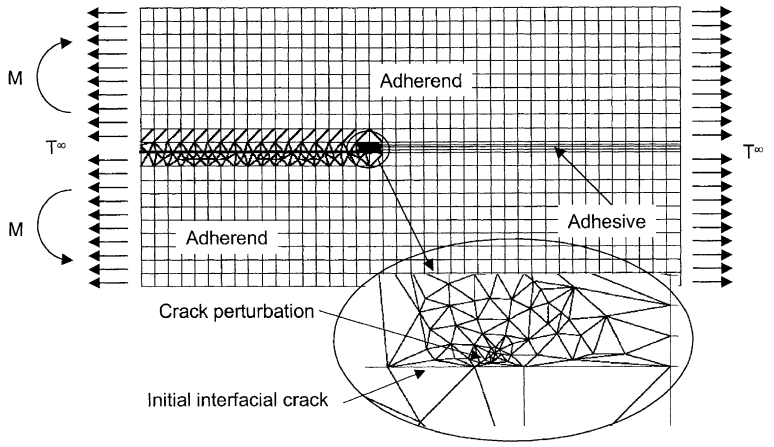

Fig. 10. The finite element mesh for predicting the crack trajectory in DCB specimen using Franc2D/L.

such a direction that the crack tends to deviate away from the interface. As the distance δt increases, the corresponding K_{II} value drops drastically, which suggests that the sub-interface crack will deviate from the interface in a rather gradual fashion. This prediction is consistent with crack trajectory shown in the SEM of the DCB specimens with directionally unstable cracks in Fig. 2. Fig. 8 also shows that if the applied strain energy release rate G increases, the K_{II} component also increases, which suggests that the sub-interface crack will deviate from the interface more quickly as G increases. Supportive information can also be found in Fleck et al. (1991). Since differences in the material mismatch will result in variations in the stress distribution, Fig. 9 also indicates that the crack propagation behavior will also be different for different materials systems, which has been further explored in Chen et al. (2001).

The analysis of the interface mechanics provided useful insights into the crack propagation behavior in adhesively bonded joints. To predict directionally unstable crack trajectories, a finite element model for the DCB specimen was constructed using Franc2D/L (Swenson and James, 1998) as shown in Fig. 10. An adhesive layer (material 2) with thickness of $t = 0.5$ mm is sandwiched between two adherends (material 1) with thickness of $H = 6$ mm, and a straight crack is located at the interface between the adhesive and the adherend. At the crack tip, there is a small crack kink into the adhesive with a length of 0.01 mm and an angle of 30° with respect to the interface. The purpose of the crack perturbation is to start the crack deviation quickly and save the simulation time. According to the interface mechanics discussed earlier, a interface crack will deviate away from the interface automatically and no crack perturbation is necessary. The displacements of one end of the model were constrained. Moments of opposite direction were applied on the other end of the adherends to simulate the external loads. A horizontal tensile stress T^{∞} was applied to achieve the desired T-stress level. Three types of elements were used in the analysis. Eight-node, plane-strain elements were used with reduced integration in the area away from the crack tip; right around the crack tip, the elements used were quarter-point singular elements; and in the area in between, triangle elements were used for the convenience of remeshing during the crack propagation. Both the adherends and adhesive were modeled as linear elastic materials with material constants $E_1 = 70$ GPa, $E_2 = 2.97$ GPa, and $v_1 = v_2 = 0.33$. The residual stress in the adhesive layer was estimated as 13 MPa and the adhesive bond was assumed to have an iso-fracture toughness value of 310 J/m^2 as discussed earlier. The interface crack with a small perturbation was assumed to be present originally in the specimen and T^{∞} was adjusted to such a value that $K_{II} = 0$ at the crack tip. This analysis intended to predict the crack trajectory as the crack advances through the following procedure:

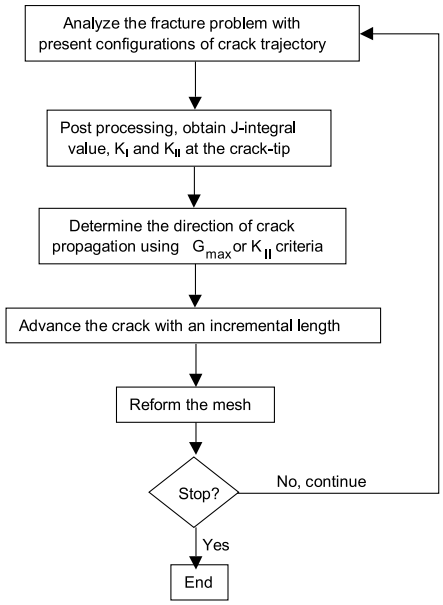

In the finite element analysis, the stress singularity at the crack tip was simulated using the quarter-point singular element, which provides a singularity with an order of $r^{-1/2}$. However, according to Cook and Ergodan (1972), the order of the stress singularity of a crack perpendicular to a bi-material interface approaches to $r^{\lambda-1}$ as the crack propagates toward the interface, where λ is determined by the material mismatch at the interface. Consequently, certain errors existed in stresses at the crack tip in the finite element analysis when the crack approached the interface. However, since only the direction of the crack propagation was of interest in this study, which was determined by the phase angle instead of the stresses, errors in the magnitude of stress singularity did not affect the result of crack trajectory.

The strain energy release rate (J-integral value) versus the normalized kinked crack length S/t is plotted in Fig. 11. The result shows that the energy available for the crack increases as the crack advances thickness-wise in the adhesive layer and decreases drastically as the crack approaches the opposite interface due to the rigid boundary of the adherend. If the crack continues to grow, the crack may possibly propagate into the adherend, kink into the interface, or reflect back to the adhesive layer. The final direction depends on the amount of energy release rate available relative to the fracture toughness of the adhesive bond in that particular direction according to the criteria of cracking direction reviewed earlier in this paper. Fig. 11 shows that the most likely scenario is for the crack to kink into the interface since more energy is available in that direction than for the other possibilities. Supportive information can also be found in He et al. (1991). A similar tendency is found in Fig. 12, where the phase angle $\psi = \tan^{-1}(K_{II}/K_I)$ at the crack tip versus the normalized kinked crack length S/t is plotted. As the crack propagates, the phase angle is negative, which indicates that the crack would propagate along a trajectory with an increasing slope. When the crack approaches the top interface, ψ increases rapidly and becomes positive at the interface, which indicates a high possibility of abrupt kink for the crack. Furthermore, the fracture toughness of adherends in adhesive bonds is normally much higher than that of adhesive, consequently, the crack will kink into the interface due the restriction of the adherends. Supportive information can also be found in He and Hutchinson (1989) where the deflection behavior of a straight crack located close to the interface of dissimilar materials is analyzed.

After kinking occurs, the crack grows along the interface. Meanwhile, the phase angle at the crack tip increases. Shown in Fig. 13 is the phase angle $\psi = \tan^{-1}(K_{II}/K_I)$ versus the normalized interfacial crack

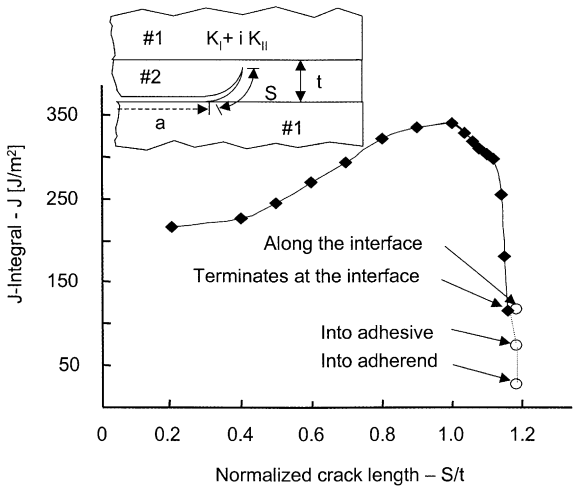

Fig. 11. Strain energy release rate (J-integral value) available at the crack tip versus the non-dimensional crack length obtained using the finite element analysis.

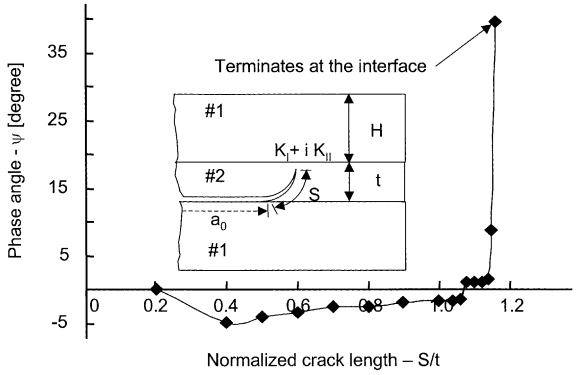

Fig. 12. Phase angle at the crack tip versus the non-dimensional crack length obtained by the finite element analysis.

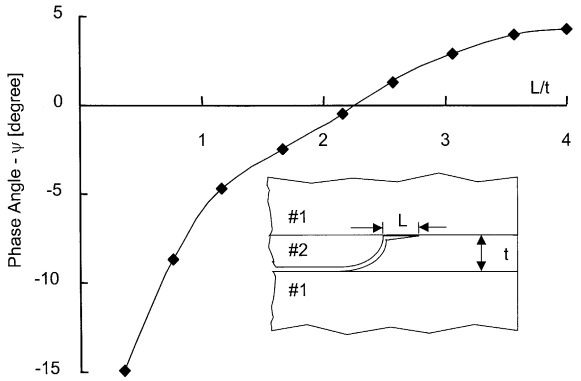

Fig. 13. Phase angle at the crack tip versus the non-dimensional interfacial crack length obtained by the finite element analysis.

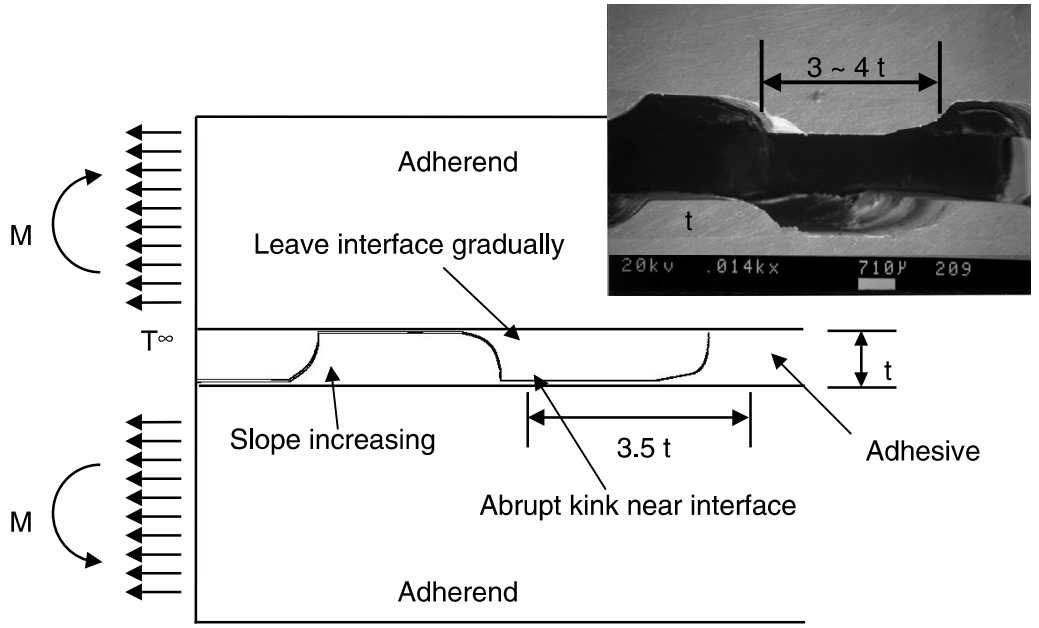

Fig. 14. The crack trajectory predicted by the finite element analysis using Franc2D/L. The result reflects the overall characteristics of the actual crack trajectory such as the characteristic length of the crack as shown in the SEM.

length L/t, where K_{II} and K_I are obtained using the sub-interface crack concept and by assuming $\delta t \ll 1$. The result suggests that after propagating along the interface for two to three times the thickness of the adhesive layer, the crack will start to leave the interface due to the increase in phase angle, which is consistent with the experimental observations of the crack trajectory shown in Fig. 2. These results are also consistent with the results discussed in Akisanya and Fleck (1992b) theoretically. However, due to the different material system treated, the results discussed in this paper appeared to be more consistent for our observations.

Fig. 14 shows the final result of the FEA simulation of the crack trajectory (the FEA mesh is hidden for a clear observation of the crack path). Compared to the SEM of the actual crack trajectory (the insert in Fig. 14), the numerical simulation accurately reproduces the characteristic length of the alternating crack of three to four times the thickness of the adhesive layer and the overall characteristic shape of the actual crack trajectory.

4. Summary and conclusions

This paper investigated directionally unstable crack propagation behavior in adhesively bonded joints. From the results, the following conclusions can be made:

(1) The directional stability of cracks in DCB specimens was predicted through analyzing the energy balance in the system. Although the simplification of the crack trajectory in the model is still crude, the error induced is negligible as far as energy balance is concerned and the results are satisfactory.

(2) The analysis of the energy balance showed that more energy becomes available for directionally unstable crack propagation as the residual stress increases, which is consistent with the results obtained using the T-stress argument by Fleck et al. (1991) and Chen and Dillard (2001).

(3) The energy model also predicted the effect of adherend bending and the effect of fracture toughness of adhesive bonds. Directionally unstable cracks are more likely to occur as the thickness of the adherend decreases whereas are less likely to occur as the fracture toughness of adhesive bonds increases.

(4) The analysis of the interface mechanics provides useful insights into the crack propagation behavior in adhesively bonded joints. Due to material mismatch, the stress at the sub-interface crack is highly mixed mode and the mode mixity decreases drastically as the distance from the crack to the interface increases, which, indicates that a sub-interface crack will deviate away from the interface in a gradual fashion. This prediction was verified by the SEM of the crack trajectory in DCB specimen with directionally unstable cracks.

(5) The finite element analysis further explored the detailed mechanics of the directionally unstable crack propagation and the predicted crack trajectory reflects the overall characteristics in the actual trajectory observed from the SEM.

Acknowledgements

The authors wish to thank the National Science Foundation-Science and Technology Center on High Performance Polymeric Adhesives and Composites at Virginia Tech (#DMR-912004) for supporting this research. The authors would also like to acknowledge the interdisciplinary forum provided by the Center for Adhesive and Sealant Science as well as facilities provided by the Engineering Science and Mechanics Department.

References

Akisanya, A.R., Fleck, N.A., 1992a. Analysis of a wavy crack in sandwich specimens. Int. J. Fract. 55, 29–45.

Akisanya, A.R., Fleck, N.A., 1992b. Brittle fracture of adhesive joints. Int. J. Fract. 58, 93–114.

Broek, D., 1982. Elementary Engineering Fracture Mechanics, Martinus Nijhoff Publishers, Alphen aan den Rijn, The Netherlands.

Chai, H., 1984. The characterization of mode I delamination failure in non-woven, multidirectional laminates. Composites 14 (4), 277–290.

Chai, H., 1986. On the correlation between the mode I fracture of adhesive joints and laminated composites. Engng. Fract. Mech. 24 (3), 413–431.

Chai, H., 1987. A note on crack trajectory in an elastic strip bounded by rigid substrates. Int. J. Fract. 32, 211–213.

Chao, Y.J., Liu, S., 1997. On the failure of cracks under mixed-mode loads. Int. J. Fract. 87, 201–223.

Chen, B., Dillard, D.A., 2001. The effect of the T-stress on the crack path selection in adhesively bonded joints. Int. J. Adhesion Adhesives, in press.

Chen, B., Dillard, J.G., Dillard, D.A., Clark, Jr., R.L., 2001. Crack path selection in adhesively bonded joints: the roles of material properties. J. Adhesion, in press.

Cook, T.S., Ergodan, F., 1972. Stresses in bonded materials with a crack perpendicular to the interface. Int. J. Engng. Sci. 10, 677–697.

Cotterell, B., Rice, J.R., 1980. Slightly curved or kinked cracks. Int. J. Fract. 16 (2), 155–169.

Dillard, D.A., Chen, B., Chang, T., Lai, Y.H., 1999a. Analysis of the notched coating adhesion test. J. Adhesion 69, 99–120.

Dillard, D.A., Chen, B., Parvatareddy, H., Lefebvre, D., Dillard, J.G., 1998. Where does it fail, and what does that mean? Proceedings of the 21st Annual Meeting of the Adhesion Society, Savannah, GA, pp. 7–9.

Dillard, D.A., Park, T.G., Zhang, H., Chen, B., 1999b. Measurement of residual stresses and thermal expansion in adhesive bonds, Proceedings of the 22nd Annual Meeting of the Adhesion Society, Adhesion Society, pp. 336–338.

Ergodan, V.F., Sih, G.C., 1963. On crack extension in plates under plane loading and transverse shear. Trans. ASME J. Bas. Engng. 85, 519–527.

Fleck, N.A., Hutchinson, J.W., Suo, Z., 1991. Crack path selection in a brittle adhesive layer. Int. J. Solids Struct. 27 (13), 1683–1703.

Goldstein, R.V., Salganik, R.L., 1974. Brittle fracture of solids with arbitrary cracks. Int. J. Fract. 10 (4), 507–523.

He, M.Y., Hutchinson, J.W., 1989. Crack deflection at an interface between dissimilar elastic materials. Int. J. Solids Struct. 25 (9), 1053–1067.

He, M.Y., Bartlett, A., Evans, A.G., Hutchinson, J.W., 1991. Kinking of a crack out of an interface: role of in-plane stress. J. Amer. Ceram. Soc. 74 (4), 767–771.

Hill, D.A., Kelly, P.A., Dai, D.N., Korsunsky, A.M., 1996. Solution of Crack Problem, the Distributed Dislocation Technique. Kluwer Academic Publishers, Dordrecht.

Hutchinson, J.W., 1968. Singular behavior at the end of a tensile crack tip in a hardening material. J. Mech. Phys. Solids 16, 13–31.

Hutchinson, J.W., Mear, M.E., Rice, J.R., 1987. Crack paralleling an interface between dissimilar materials. J. Appl. Mech. 54, 828–832.

Hutchinson, J.W., Suo, Z., 1992. Mixed mode cracking in layered materials. Adv. Appl. Mech. 29, 63–191.

Lasson, S.G., Carlsson, A.J., 1973. Influence of non-singular stress terms and specimen geometry on small-scale yielding at crack tips in elastic–plastic materials. J. Mech. Phys. Solids 21, 263–277.

Nairn, J.A., 1989. The strain energy release rate of composite microcracking: a variational approach. J. Compos. Mater. 23, 1106–1129.

Palaniswamy, K., Knauss, W.G., 1978. On the problem of crack extension in brittle solids under general loading. In: S. Nemat-Nasser (Ed.), Mechanics Today, vol. 4, Pergamon Press, Oxford, pp. 87–148.

Rice, J.R., 1968. A path independent integral and the approximate analysis of strain concentration by notches and cracks. J. Appl. Mech. 35, 379–386.

Suga, T., Elssner, E., Schmander, S., 1988. Composite parameters and mechanical compability of material joints. J. Compos. Mater. 22, 917–934.

Suo, Z. 1990. Failure of brittle adhesive joints. Appl. Mech. Rev. 43 (5), Part 2, S276-S279.

Suo, Z., Hutchinson, J.W., 1989. Sandwich test specimens for measuring interface crack toughness. Mater. Sci. Engng. A 107, 135–143.

Swenson, D., James, M., 1998. A crack propagation simulator for plane layered structures, Franc2D/L, version 1.4, Kansas State University, Manhattan, Kansas, USA.

Tada, H., Paris, P.C., Irwin, H.R., 1985. The Stress Analysis of Cracks Handbook. Del Research Corporation, Hellertown, Pennsylvania.

Westergaard, H.M., 1939. Bearing pressures and cracks. J. Appl. Mech. 6, 37–64.

Williams, M.L., 1957. On the stress distribution at the base of a stationary crack. J. Appl. Mech. 24, 109–114.

Williams, M.L., 1959. The stress around a fault or crack in dissimilar media. Bull. Seismol. Soc. Amer. 49 (2), 199–204.

Zhu, X.K., Chao, Y.J., 2001. Constraint effects on crack-tip fields in elastic-perfectly plastic materials. J. Mech. Phys. Solids 49, 363–399.